

## Ultrafast MAS Solid-State NMR Permits Extensive $^{13}\text{C}$ and $^1\text{H}$ Detection in Paramagnetic Metalloproteins

Ivano Bertini,<sup>\*,†,‡</sup> Lyndon Emsley,<sup>§</sup> Moreno Lelli,<sup>†</sup> Claudio Luchinat,<sup>†,‡</sup> Jiafei Mao,<sup>†</sup> and Guido Pintacuda<sup>§</sup>

Magnetic Resonance Center, CERM, University of Florence, Sesto Fiorentino, Italy, Department of Chemistry, University of Florence, Sesto Fiorentino, Italy, and Centre de RMN à Très Hauts Champs, Université de Lyon (CNRS/ENS Lyon/UCB Lyon 1), 69100 Villeurbanne, France

Received January 15, 2010; E-mail: ivanobertini@cerm.unifi.it

Solid-state NMR (ssNMR) has significantly grown in recent years thanks to combined progress in sample preparation, probe and magnet technology, and *rf* irradiation schemes, and the field is now open to the structural characterization of systems highly pertinent in many areas of modern biology.<sup>1</sup> So far, these techniques have been used on paramagnetic proteins with some success, reducing significantly the sphere of observation close to the metal center with respect to solution studies.<sup>2</sup> However, in all these studies, the coordination sphere of the metal center remains elusive. In parallel, impressive progress has shown that the use of very fast (>30 kHz) MAS allows efficient detection of previously unobservable nuclei in highly paramagnetic materials<sup>3</sup> and that this discloses a rich amount of information that can be directly linked to the electronic and molecular structure.<sup>4</sup> We show here that by using ultrafast (60 kHz) MAS on the Co<sup>II</sup>-replaced catalytic domain of matrix metalloproteinase 12 (CoMMP-12)<sup>5</sup> we can observe and assign, in a highly paramagnetic protein in the solid state, resonances from the residues coordinating the metal center. In addition, by exploiting the enhanced relaxation caused by the paramagnetic center and the low power irradiation enabled by the fast MAS, this can be achieved in remarkably short times, with only less than 1 mg of sample. Furthermore, using the known crystal structure of the compound and the assignment of ZnMMP-12,<sup>6</sup> we are able to distinguish and measure pseudocontact contributions to the shifts (PCS) up to the coordinating ligands, opening the way to unveil information on the electronic state of the coordination sphere.

Figure 1a shows the  $^{13}\text{C}$  CP spectrum of microcrystalline CoMMP-12 acquired at 22 kHz MAS at 20.0 T. The spectrum was unambiguously assigned using multidimensional  $^{13}\text{C}$ ,  $^{13}\text{C}$  and  $^{13}\text{C}$ ,  $^{15}\text{N}$  correlations to provide hundreds of PCS,<sup>7</sup> which can be used as restraints in the structure determination increasing the accuracy of the resulting structures.<sup>8</sup> However, spins close to the metal experience large highly anisotropic paramagnetic chemical shifts (a dipolar anisotropy of  $\sim 250$  ppm is estimated for nuclei at 5 Å from the Co<sup>II</sup> ion). Observing them is a very complex challenge, especially at high magnetic fields, in terms of both sensitivity (their intensity is distributed over many spinning sidebands) and resolution (the coupling to proton spins with large shift anisotropy is not well averaged by common *rf* heterodecoupling schemes). In the case of Co<sup>II</sup> (electron spin  $S = 3/2$ ), at  $\sim 20$  T and under moderate MAS regimes, correlations between  $^{13}\text{C}$  nuclei closer than 10 Å to the metal escape detection.<sup>2b,7</sup>

To counter these problems, the advantage of ultrafast MAS is twofold. First, a  $^{13}\text{C}$  CP spectrum of comparable quality can be acquired at 60 kHz MAS (Figure 1b) on a much smaller amount of sample ( $\sim 1$  mg vs 15 mg), since the interscan delay can be reduced by exploiting both the short  $^1\text{H}$  longitudinal relaxation times

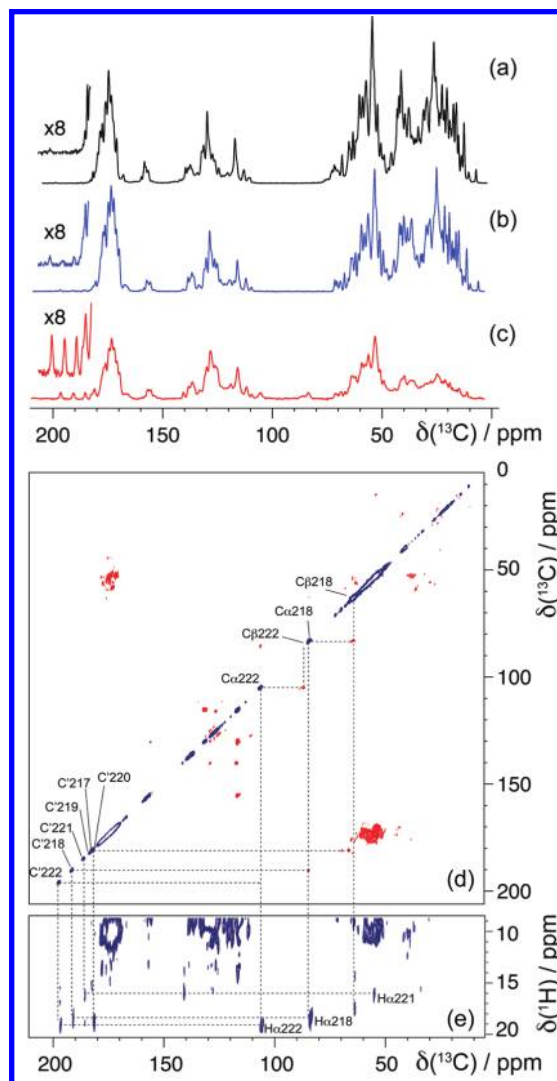


**Figure 1.** (a–c)  $^{13}\text{C}$  spectra of microcrystalline ( $^{15}\text{N}$ ,  $^{13}\text{C}$ )-labeled CoMMP-12 recorded (a) at 22 kHz MAS at 20 T ( $\omega_{\text{OH}} = 850$  MHz,  $^1\text{H}$  carrier at 7.4 ppm, 10k scans, 3 s interscan delay, total time = 15 h) and (b–c) at 60 kHz MAS at 21.2 T ( $\omega_{\text{OH}} = 900$  MHz,  $^1\text{H}$  carrier at 1.5 and 18.25 ppm, respectively, 10k scans, 2 and 0.2 s interscan delay, respectively, total times = 15 and 4 h); note that sharp diamagnetic signals in c are suppressed with respect to b. (d–e) Regions of DREAM and HETCOR correlations at 60 kHz MAS at 21.2 T.

induced by the Co<sup>II</sup> and the low-power CP and low-power decoupling allowed by ultrafast spinning.<sup>9</sup>

Second, and more importantly, as shown recently<sup>10</sup> the ultrafast MAS regime alleviates the deleterious consequences of the large anisotropy, even at very high field, because (i)  $^{13}\text{C}$  signals are now

<sup>†</sup> CERM, University of Florence.

<sup>‡</sup> Department of Chemistry, University of Florence.

<sup>§</sup> Université de Lyon.

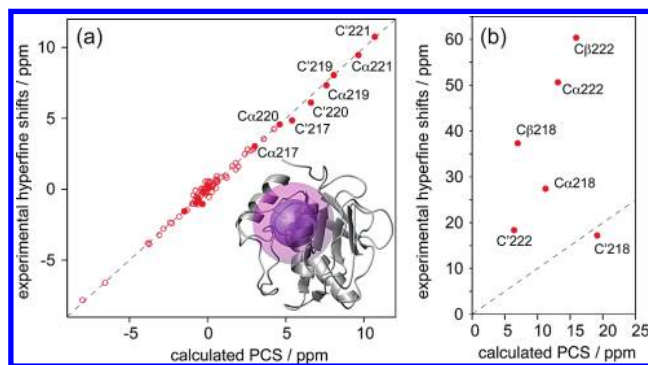


**Figure 2.** Experimental hyperfine shifts vs calculated PCS for newly assigned  $^{13}\text{C}$  spins: (a) nuclei of the metal binding loop, up to 6.2 Å; (b) nuclei from the coordinating histidines. Filled circles indicate resonances detectable at 60 kHz MAS only. The cartoon shows the blind spheres around the  $\text{Co}^{\text{II}}$  at 22 and at 60 kHz (larger and smaller sphere, respectively; see also Figure S3).

concentrated into fewer sidebands and (ii) MAS can efficiently average out the heteronuclear dipolar coupling since the large shift spreading due to paramagnetic interactions reduces the flip-flop terms between protons. This brings a consequent increase in resolution, sensitivity, and coherence lifetimes  $T_2'$  of  $^{13}\text{C}$  (and  $^1\text{H}$ ) spins. Here several new signals become clearly visible at 60 kHz MAS (Figure 1c), in the region around 200 and 100 ppm. These resonances can be selectively enhanced by optimizing the recycle times between scans and saturating the resonances of the “diamagnetic” nuclei and by setting the  $^1\text{H}$  carrier either upfield or downfield of the diamagnetic region so as to minimize off-resonance effects on largely shifted resonances.

Furthermore, solid-state signals are not subject to Curie broadening:<sup>10</sup> the long coherence lifetimes are essential to the realization of the  $^1\text{H}$ – $^{13}\text{C}$  coherence transfers used here, and the metal center does not significantly reduce the efficiency of magnetization transfer. Dipolar-based experiments optimized for the fast MAS regime (double quantum CP,<sup>9c</sup> DREAM<sup>11</sup>) thus provide efficient ways to generate correlations between these spins, similar to diamagnetic materials (Figure 1d).

Finally, the strongly shifted paramagnetic resonances allow the exploitation of the proton dimension for resonance assignment, traditionally inaccessible in solid diamagnetic proteins, but already exploited in the investigation of small paramagnetic complexes.<sup>3,4</sup> Several well resolved proton resonances correlate with nearby  $^{13}\text{C}$  spins in 2D  $^1\text{H}$ – $^{13}\text{C}$  HETCOR experiments (downfield region reported in Figure 1e; full spectra in Supporting Information (SI)). In total, 88 new signals can be recorded by the combined resolution offered by high field and high rates, and in particular six new spin systems can be identified in the 1D  $^{13}\text{C}$  CP and 2D HETCOR and DREAM spectra. Assignment can be performed on the basis of the available X-ray structure of ZnMMP-12<sup>6a</sup> (PDB: 1RMZ) and of the magnetic susceptibility tensor parameters fitted to the PCS values measured far from the metal center. By comparing the results of the calculation to the observed NMR shifts, the best assignment (Figure 2a) minimizes the squared deviation of each group of signals within the same spin system. With this assignment, the PCS match the calculated values for nuclei as close as 6.2 Å to the metal, i.e. located in the metal binding loop and just before and after the coordinating histidines.

As a first result, this larger set of PCS can be used to refine the magnitude and orientation of the magnetic susceptibility tensor, together with the metal position, with respect to the protein backbone, to yield in turn more precise structural restraints. This procedure was performed including the simultaneous adjustment

of all the neighboring metals in the crystal lattice and fulfilling the crystallographic symmetry. The refined paramagnetic tensor values (see SI) allow us to find a  $\text{Co}^{\text{II}}$  position closer ( $0.13 \pm 0.09 \text{ \AA}$  vs  $0.30 \text{ \AA}$ <sup>7</sup>) to the crystallographic position of  $\text{Zn}^{\text{II}}$  in MMP-12.

As a second result, we observe that six additional resonances (corresponding to two independent spin systems), downfield shifted in the  $^{13}\text{C}$  CP spectrum, deviate substantially from predicted values (Figure 2b). These resonances can be reasonably assigned to the C', C $\alpha$ , and C $\beta$  spins of two coordinating histidines, nuclei for which the point–dipole approximation underlying the functional form of the PCS starts breaking down, and a large portion of the paramagnetic shift is likely to result from the direct delocalization of the metal unpaired electrons (contact shift). The differences between experimental shifts and the expected PCS values may thus provide here access to the distribution of  $\text{Co}^{\text{II}}$  spin density in this metalloenzyme.

In conclusion, the use of ultrafast MAS and low-power decoupling/fast recycling protocols allows us to detect and assign nuclei as close as 5.6 Å from the  $\text{Co}^{\text{II}}$  in MMP-12, opening the way to ssNMR characterization of the metal coordination environment in metalloproteins and in general of any immobilized systems containing paramagnetic ions.

**Acknowledgment.** Support from the Agence Nationale de la Recherche (ANR 08-BLAN-0035-01), from Ente Cassa di Risparmio di Firenze, and from JRA and Access to Infrastructures activity in the 6th FP of the EC (RII3-026145, EU-NMR).

**Supporting Information Available:** Experimental details, full spectra, comparison between  $^{13}\text{C}$ ,  $^{13}\text{C}$  correlations at two different fields, and assigned PCS. This material is available free of charge via the Internet at <http://pubs.acs.org>.

## References

- (1) McDermott, A. E. *Curr. Opin. Struct. Biol.* **2004**, *14*, 554–561. (b) Lange, A.; Giller, K.; Hornig, S.; Martin-Eauclaire, M. F.; Pongs, O.; Becker, S.; Baldus, M. *Nature* **2006**, *440*, 959–962. (c) Wasmer, C.; Lange, A.; Van Melckebeke, H.; Siemer, A. B.; Riek, R.; Meier, B. H. *Science* **2008**, *319*, 1523–1526. (d) Böckmann, A. *Angew. Chem., Int. Ed.* **2008**, *47*, 6110–6113. (e) Bayro, M. J.; Maly, T.; Birkett, N. R.; Dobson, C. M.; Griffin, R. G. *Angew. Chem., Int. Ed.* **2009**, *48*, 5708–5710.
- (2) Pintacuda, G.; Giraud, N.; Pierattelli, R.; Bockmann, A.; Bertini, I.; Emsley, L. *Angew. Chem., Int. Ed.* **2007**, *46*, 1079–1082. (b) Balayssac, S.; Bertini, I.; Lelli, M.; Luchinat, C.; Maletta, M. *J. Am. Chem. Soc.* **2007**, *129*, 2218–2219. (c) Nadaud, P. S.; Helmus, J. J.; Kall, S. L.; Jaroniec, C. P. *J. Am. Chem. Soc.* **2009**, *131*, 8108–8120.
- (3) (a) Ishii, Y.; Wickramasinghe, N. P.; Chimon, S. *J. Am. Chem. Soc.* **2003**, *125*, 3438–3439. (b) Wickramasinghe, N. P.; Shaibat, M. A.; Jones, C. R.; Casabianca, L. B.; de Dios, A. C.; Harwood, J. S.; Ishii, Y. *J. Chem. Phys.* **2008**, *128*, 52210–52215.
- (4) (a) Kervern, G.; Pintacuda, G.; Zhang, Y.; Oldfield, E.; Roukoss, C.; Kuntz, E.; Herdtweck, E.; Basset, J. M.; Cadars, S.; Lesage, A.; Coperet, C.; Emsley, L. *J. Am. Chem. Soc.* **2006**, *128*, 13545–13552. (b) Huang, W.; Schöpfer, M.; Zhang, C.; Howell, R. C.; Todaro, L.; Gee, B. A.; Francesconi, L. C.; Polenova, T. *J. Am. Chem. Soc.* **2008**, *130*, 481–490. (c) Kervern, G.; D'Aleo, A.; Toupet, L.; Maury, O.; Emsley, L.; Pintacuda, G. *Angew. Chem., Int. Ed.* **2009**, *48*, 3082–3086.
- (5) Bertini, I.; Fragai, M.; Lee, Y. M.; Luchinat, C.; Terni, B. *Angew. Chem., Int. Ed.* **2004**, *43*, 2254–2256.
- (6) (a) Bertini, I.; Calderone, V.; Cosenza, M.; Fragai, M.; Lee, Y. M.; Luchinat, C.; Mangani, S.; Terni, B.; Turano, P. *Proc. Natl. Acad. Sci. U.S.A.* **2005**, *102*, 5334–5339. (b) Balayssac, S.; Bertini, I.; Falber, K.; Fragai, M.; Jehle, S.; Lelli, M.; Luchinat, C.; Oschkinat, H.; Yeo, K. J. *ChemBioChem* **2007**, *8*, 486–489.
- (7) Balayssac, S.; Bertini, I.; Bhaumik, A.; Lelli, M.; Luchinat, C. *Proc. Natl. Acad. Sci. U.S.A.* **2008**, *105*, 17284–17289.
- (8) Bertini, I.; Bhaumik, A.; De Paëpe, G.; Griffin, R. G.; Lelli, M.; Lewandowski, J. R.; Luchinat, C. *J. Am. Chem. Soc.* **2010**, *132*, 1032–1040.
- (9) (a) Laage, S.; Marchetti, A.; Sein, J.; Pierattelli, R.; Sass, H. J.; Grzesiek, S.; Lesage, A.; Pintacuda, G.; Emsley, L. *J. Am. Chem. Soc.* **2008**, *130*, 17216–17217. (b) Wickramasinghe, N. P.; Parthasarathy, S.; Jones, C. R.; Bhardwaj, C.; Long, F.; Kotecha, M.; Mehboob, S.; Fung, L. W.; Past, J.; Samoson, A.; Ishii, Y. *Nat. Methods* **2009**, *6*, 215–218. (c) Laage, S.; Sachleben, J. R.; Steuernagel, S.; Pierattelli, R.; Pintacuda, G.; Emsley, L. *J. Magn. Reson.* **2009**, *196*, 133–141.
- (10) Kervern, G.; Steuernagel, S.; Engelke, F.; Pintacuda, G.; Emsley, L. *J. Am. Chem. Soc.* **2007**, *129*, 14118–14119.
- (11) Verel, R.; Ernst, M.; Meier, B. H. *J. Magn. Reson.* **2001**, *150*, 81–99. JA100398Q